

Catalytic transformation of ethanol to methane and butene over NiO NPs supported over mesoporous SBA-15

Sauvik Chatterjee^a, Kushanava Bhaduri^b, Arindam Modak^a, Manickam Selvaraj^c,
Rajaram Bal^d, Biswajit Chowdhury^{b,*}, Asim Bhaumik^{a,*}

^a School of Materials Sciences, Indian Association for the Cultivation of Science, Jadavpur, Kolkata, 700 032, India

^b Department of Chemistry, Indian Institute of Technology (ISM), Dhanbad, Dhanbad 826004, Jharkhand, India

^c Department of Chemistry, Faculty of Science, King Khalid University, Abha 61413, Saudi Arabia

^d Nanocatalysis Area, Light Stock Processing Division, CSIR-Indian Institute of Petroleum, Dehradun 248005, Uttarakhand, India

ARTICLE INFO

Keywords:

Mesoporous SBA-15
Immobilization of NiO NPs
Dehydrogenation of ethanol
Hydrocarbon fuels
Hydrogen production

ABSTRACT

Hexagonally ordered mesoporous silica material SBA-15 with thick pore wall is an ideal catalytic support for immobilizing reactive tiny metal oxide nanoparticles (NPs) due to its large pore size, high specific surface area, excellent feasibility for the immobilization of NPs and robust nature of the mesoporous framework. NiO@SBA-15 nanocomposite material has been synthesised through non-ionic surfactant assisted hydrothermal synthesis of SBA-15 followed by calcination, functionalization and impregnation. The material has been thoroughly characterized by using powder XRD, N₂ sorption, XPS and NH₃-TPD. NiO@SBA-15 with ca. 13 % Ni(II) loading displayed specific surface area of 409 m² g⁻¹ and weak surface acidity. NiO@SBA-15 showed good catalytic activity for conversion of ethanol to hydrocarbon fuels, specifically C1 and C4 hydrocarbons at 300 °C together with the production of hydrogen in almost stoichiometric amount. Further increase in the reaction temperature favoured cracking to yield methane as the major product. Supported NiO NPs acts as efficient catalytic centre for the conversion of ethanol to hydrocarbon fuels, which is an alternate to fossil fuel. Catalytic process is environment friendly and sustainable as the feedstock ethanol can be easily obtained from biomass resources.

Introduction

In the backdrop of global energy scenario, conversion of biomass derived abundant resources like ethanol to hydrocarbon fuels is becoming increasingly demanding in the field of energy research [1]. Ethanol derived from natural sources like sugarcane [2] is an excellent platform chemical for various value added chemicals such as isopropanol, ethylene, 1,3-butadiene, 2-butene, acetaldehyde and many more [3]. However, ethanol can be used only as an additive to gasoline for achieving high torque and output power in comparison to gasoline alone engine. It suffers from the major disadvantage of low net calorific value [4]. Often it can be considered as a replacement of fossil fuel as a gasoline component [5–8]. However, direct utilization of ethanol as fuel is not feasible in existing motorization technique [5,7]. Hence, one step up-gradation can be considered as a good attempt to convert the large volume of ethanol supply chain into fuel with low carbon count. In this viewpoint a new approach of research has been conducted to boost up the valuation of ethanol by using it as a starting material for direct

synthesis of hydrocarbon fuels [3,9]. This will also be an additional relief in the context of fast diminishing fossil fuels. Moreover, hydrogen is also produced as one of the major products in the ethanol dehydrogenation process. Hydrogen is recognized as an alternative energy carrier for attaining a low carbon economy and excellent sustainability in the supply of energy [10,11]. However, hydrogen is mostly produced via biomass gasification or methane reforming [12], which are energy consuming and involved complex catalytic processes. Hence, in this scenario H₂ production via ethanol transformation can make a credible alternative as it is produced from biomass fermentation [13] without applying any additional energy. In this way abundant biomass can be efficiently utilized, which in return make the hydrogen production much cheaper. This altogether fulfils the idea of integrated refining of biomass for sustainable energy [14–16].

Porous inorganic nanomaterials have long been considered as attractive heterogeneous catalyst because of their high specific surface area, tuneable porosity and ease of stabilization of the metal/metal oxide NPs at its pore surface [17–20]. Amongst them mesoporous silica

* Corresponding authors.

E-mail addresses: biswajit72@iitism.ac.in (B. Chowdhury), msab@iacs.res.in (A. Bhaumik).

<https://doi.org/10.1016/j.mcat.2020.111381>

Received 16 September 2020; Received in revised form 23 December 2020; Accepted 24 December 2020

Available online 18 January 2021

2468-8231/© 2021 Elsevier B.V. All rights reserved.

has been intensively studied as support for designing reactive heterogeneous catalysts [21–27]. Owing to very high BET surface area the 2D-hexagonal mesoporous silica materials are often used as support for surface functionalization as well as immobilizing active catalytic sites. Large mesopores of the functionalized SBA-15 is found to be very efficient for loading of metal and metal oxide NPs [28–31]. This in turn could facilitate the catalytic activity by easy diffusion of reactant and products along the pore channels. For achieving high conversion in ethanol to gasoline, H-ZSM-5 has been employed as catalyst under fixed-bed reaction conditions [32–34]. On the other hand enhancement of the catalytic activity of ZSM-5 in the conversion of ethanol to ethylene and subsequent higher hydrocarbons has been the underway for several decades [35,36]. The acid site of ZSM-5 catalyses the poly-alkylation and cracking to produce C_3+ hydrocarbons and olefins. The hydrocarbon efficiency can be enhanced by increasing the metallic sites in the zeolitic support [37]. While the acidic site of the H-ZSM-5 enhances the protonation of the alcohol and subsequent dehydration, metal centre present in the framework act as a dehydrogenating cum coupling agent to form higher olefins. Hence by eliminating acidic centre from the support the olefin pool may be enhanced. Thus, SBA-15 with very mild acidity [38] is quite good support for the metal oxides to convert ethanol into a hydrocarbon pool having high fuel efficiency.

Here we have supported NiO NPs over functionalized 2D-hexagonal mesoporous SBA-15 material followed by calcination in air to obtain NiO@SBA-15 material. NiO@SBA-15 acts as an efficient catalyst for the dehydrogenation of ethanol to a mixture of methane and butane isomers. NiO@SBA-15 has been synthesized by surface modification of SBA-15 followed by immobilization of Ni(II) at its surface and calcination (Scheme 1). NiO@SBA-15 showed good catalytic activity for conversion of ethanol to a mixture of hydrocarbons, specifically C1 and C4 hydrocarbons at mere 300 °C reaction temperature under fixed-bed reaction conditions. Further increase in the reaction temperature favoured cracking to yield CH_4 as major product.

Results and discussion

Powder XRD analysis

The mesophase of NiO@SBA-15 has been characterized through the powder XRD analysis (Fig. 1). The PXRD data for SBA-15 showed only broad hump at 24° 2θ region (Fig. 1B, left) due to amorphous thick silica pore wall. After the loading of NiO NPs we got additional peaks at 37° , 43° and 63° 2θ , which suggested the presence of (111), (200) and (220) planes for NiO nanoparticles as per the JCPDS card No. 47-1049 (Fig. 1A) [39]. To understand the periodicity of the material small angle PXRD pattern has been recorded. There we observe consecutive shift in peaks towards lower 2θ value upon each step of surface

modification. In case of NiO@SBA-15 (100), (110) and (200) peaks are recorded at 1.01° , 1.71° and 1.96° degrees of 2θ . For pure silica SBA-15 material the peaks appeared at 0.96° , 1.63° and 1.88° degrees of 2θ respectively. This result agrees well with 2D-hexagonally ordered SBA-15 material (Fig. 1B, right) [40,41]. The shift in the peak positions indicated the decrease in d-spacing upon functionalization and NiO loading. The Scherrer's equation has been employed to estimate the average particle size of the NiO nanoparticles. The average particle size NiO NPs by using this method was found to be ca. 5.2 nm.

Surface area analysis

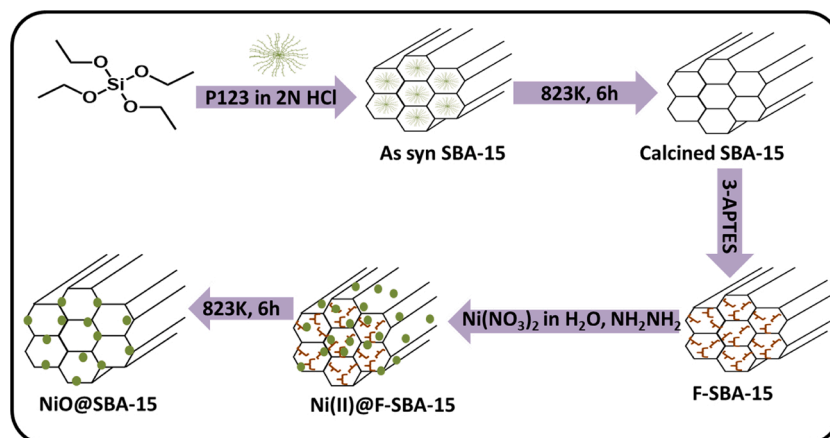
To understand the porosity and BET surface area of NiO@SBA-15 the N_2 adsorption-desorption analysis has been performed at 77 K. The N_2 sorption isotherms shown in Fig. 2 displayed a typical type IV isotherm together with a H1 type hysteresis loop indicative of presence of large mesopore, characteristics of SBA-15 type framework [42]. Significant drop in BET surface area was observed when SBA-15 was first functionalized with APTES followed by loading of NiO. In the case of SBA-15 the observed specific surface area was $872\text{ m}^2\text{ g}^{-1}$, whereas in case of NiO@SBA-15 the same was found to be $409\text{ m}^2\text{ g}^{-1}$. The pore size distribution shown in the inset of Fig. 2 suggested the presence of broad mesopore with peak pore width of 6.5–7.2 along with some micropore of ca. 1.1 nm size in the NiO@SBA-15 sample. The mesopore size corresponds to the 2D-hexagonal mesophase of SBA-15 framework, whereas the micropore contribution could be attributed to some porosity in the amorphous pore wall.

X-ray photoelectron spectroscopic analysis

X-ray photoelectron spectroscopic analysis have been carried out for NiO@SBA-15 to understand the oxidation state of Ni present in the material after calcination. Peaks observed at 104 and 533 eV could be assigned due to the binding energies of the Si 2p (Fig. 3A) and O 1s (Fig. 3B) electrons present in the mesoporous silica framework [43]. The binding energy for Ni 2p $_{3/2}$ state was found to be at 857 eV with its satellite peak at 863 eV, which confirms that the Ni present in material is exclusively in +2 oxidation state (Fig. 3C) [44]. XPS spectra has been quantitatively analysed and it suggested loading of Ni in the material was 13.67 wt%. High loading of Ni in NiO@SBA-15 nanocatalyst in turn is helpful for carrying out the catalytic reaction under fixed-bed reaction conditions.

Morphological study

To understand the morphological features scanning electron microscopic and transmission electron microscopic images were recorded. The



Scheme 1. Schematic synthesis pathway for NiO@SBA-15.

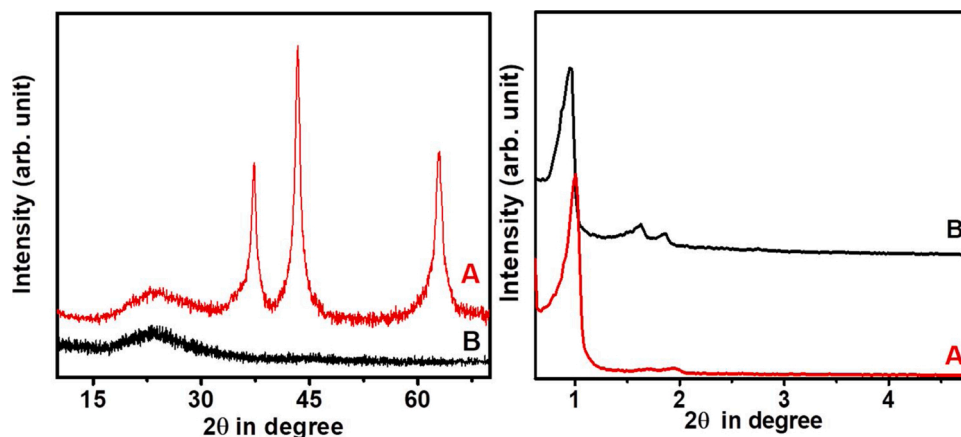


Fig. 1. Wide angle (left) and small angle (right) PXRD for NiO@SBA-15 (A) and pure silica SBA-15 (B).

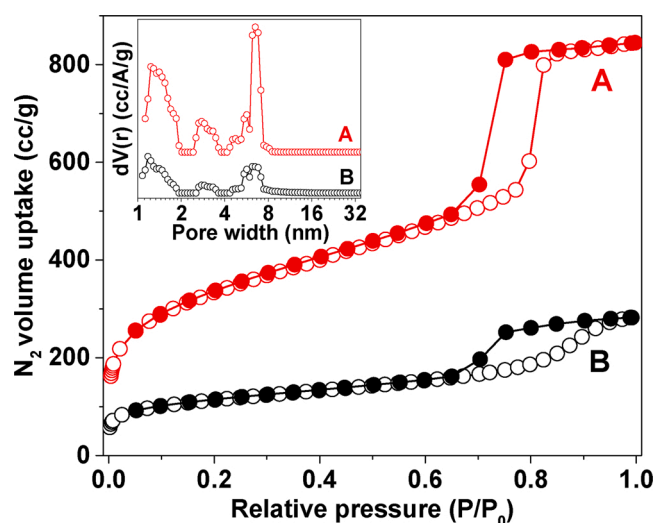


Fig. 2. N_2 adsorption-desorption isotherm for SBA-15 (A) and NiO@SBA-15 (B); Pore size distribution for SBA-15 (A) and NiO@SBA-15 (B) in the inset.

SEM images reveal the materials are arranged like the fish gill like orderly array (Fig. 4a). Elemental mapping images showed the NiO nanoparticles are distributed uniformly (Fig. 4b, c and d). The high resolution SEM image (Figure S1) shows the presence of periodic channels which was also confirmed from the HR TEM image (Fig. 4e, f). This HR TEM image of NiO@SBA-15 suggested the tiny NiO nanoparticles of dimension ca. 5–6 nm are uniformly distributed throughout the material. Further, the HR TEM images confirmed the pore width of

ca. 7 nm in NiO@SBA-15. It is pertinent to mention that functionalization with 3-aminopropyl groups provides specific metal binding sites at the mesopore surface, so that the Ni(II) ions can evenly dispersed across the support. This helps in the formation of very small dimension NiO nanoparticle upon calcination. TEM images and elemental mapping data suggested that NiO NPs are well dispersed throughout the NiO@SBA-15 material and NiO NPs are located both inside the pore channel as well as outside the pores.

Surface acidity measurement

To understand the surface acidity, temperature programmed desorption of ammonia experiment has been carried out from 298 to 1073 K for NiO@SBA-15 material. It is observed that the sharp peak at lower temperature range 313–498 K is (12.4 mL/g or 0.5549 mmol/g Fig. 5) and this could be attributed to the weak acid sites present in the material. On the other hand, two broad peaks in the temperature range 512–1073 K is observed. These broad peaks are deconvoluted to understand the contribution of each peaks. These high temperature NH_3 desorption peaks could be attributed to the presence of the medium and strong acidic sites. It is seen that the peak appeared in the temperature range 512–783 K corresponds to moderate acidity with acidity of 0.475 mmol/g and the one observed in the temperature range 793–1073 K could be assigned due to strong acidity with total concentration of 0.55089 mmol/g. In Fig. 5b we have shown the strengths of different acid sites through bar diagram.

Catalytic activity

Catalytic transformation of ethanol has been carried out over NiO@SBA-15 in the temperature range 300–400 °C. In Table 1 we have

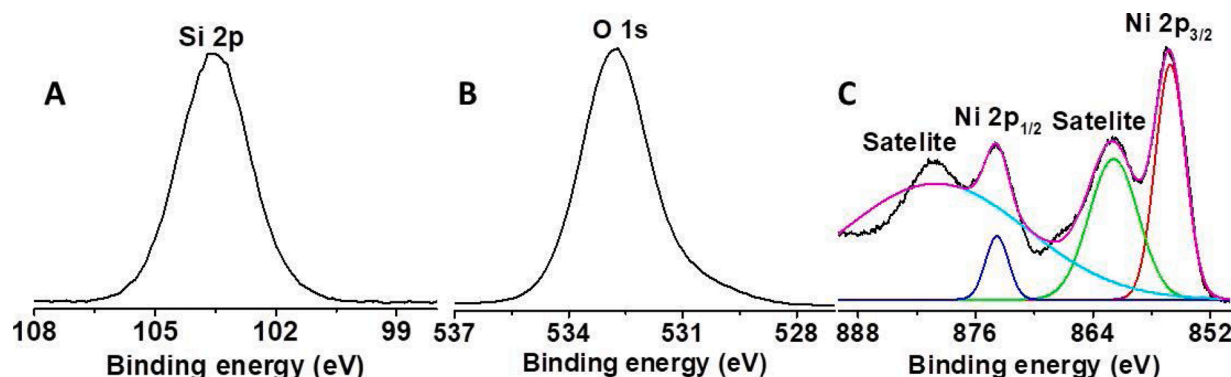


Fig. 3. Short range XPS scan of NiO@SBA-15 for the Si (A), O (B), Ni (C).

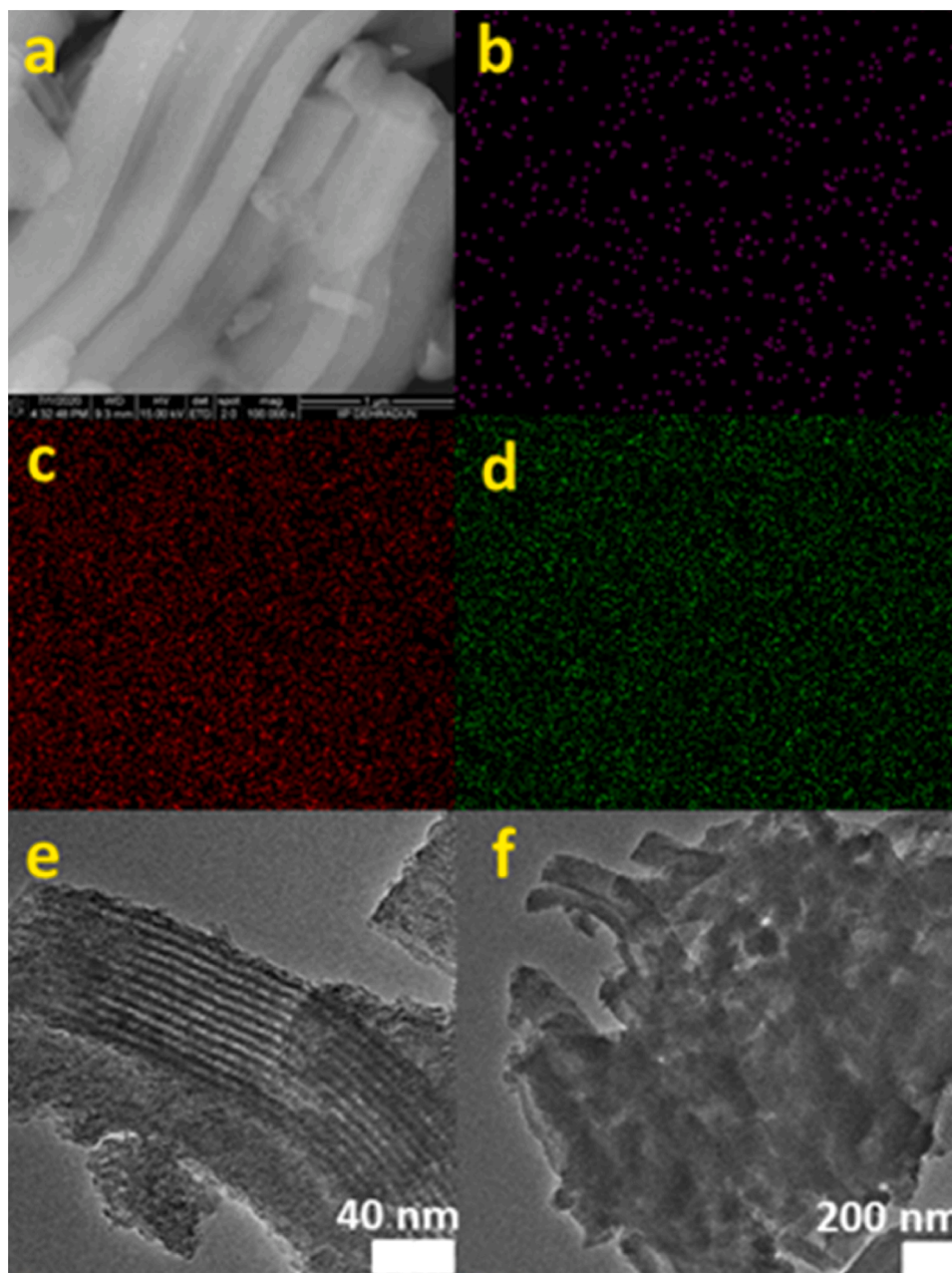
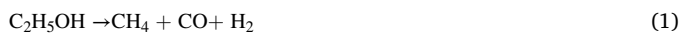


Fig. 4. FE-SEM image of NiO@SBA-15 (a), its elemental mapping for Ni (b), Si (c), O (d); and HR TEM images (e,f) at different magnifications.

summarized the yields of different products over NiO@SBA-15 catalyst at different temperatures. At 300 °C the ethanol conversion was rather low but formation of methane and butene occurs predominantly along with ethylene, diethyl ether and trace amount of other hydrocarbons. Further we could detect small amount of benzene also at 300 °C. However, with increase in temperature to 350 °C we can see the ethanol conversion increases considerably and further at 400 °C a near complete conversion of ethanol was observed. Among the hydrocarbons high amount of CH₄ was observed at higher temperature and selectivity to C₂-C₄ were found in trace amount (Fig. 6). At higher temperature C—C bond breaking occurs by the following step at the NiO@SBA-15 surface (Eq. (1)).



At low temperature it was previously observed that comparatively large amount of high molecular weight hydrocarbons are formed, which could diffuse through the mesoporous pore channels of the catalyst and

this leads to reduced coke deposition on the catalyst surface.¹ It is interesting to note that substantial amount of hydrogen was detected in all temperatures. The production of hydrogen can be explained mainly on the basis of cracking and ethanol steam reforming (ESR) at high temperatures. Further, high yield of methane could be attributed to the methanation of ESR product (Eqs. (1)–(5)) [45].



During regeneration more methane was formed along with hydrogen, which indicated more decomposition/cracking of ethanol (Table S1). However, among the lower hydrocarbon products C₄ fractions were obtained predominantly compare to C₁-C₃ fractions (Fig. 6).

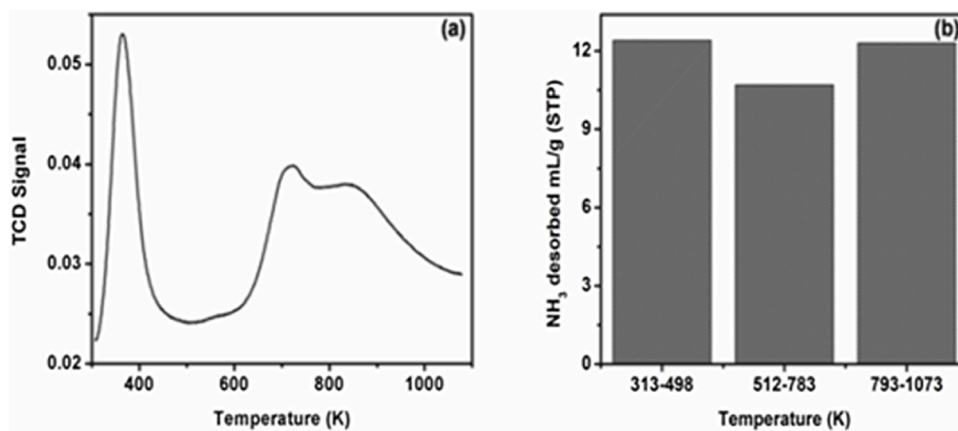


Fig. 5. NH_3 -TPD profile (a) and amount of NH_3 (mL/g) desorbed (b) over NiO@SBA-15.

Table 1

Optimization of NiO@SBA-15 catalyst at different temperatures for the transformation of ethanol.

Temp. ($^{\circ}\text{C}$)	TOS (h)	Ethanol Conv.%	Selectivity (%)									Carbon Balance (%)
			CH_4	C_2H_4	C_2H_6	C_3H_6	C_3H_8	C_4H_8	DEE	C_6H_6	H_2	
300	1	39.4	8.7	0.3	0	0	0.7	8	0.3	trace	21.1	71.5
	2	28.1	13	0.4	0	0	0.9	10.1	0.5	trace	29.6	82.5
	3	30.3	10.9	0.3	0	0	0.7	8.2	0.4	trace	22.8	79.2
	4	29.8	11	0.3	0	0	0.7	7.9	0.4	trace	21.6	79.4
	5	33.3	9.5	0.3	0	0	0.5	6.9	0.4	trace	18.4	75.6
	6	30.3	10.5	0.3	0	0	0.7	7.6	0.4	trace	20.3	78.7
	7	24.8	12.6	0.4	0	0	0.9	8.9	0.5	trace	24.4	84.0
	8	26.3	11.7	0.3	0	0	0.8	8.4	0.4	trace	22.5	82.3
350	1	80.2	45.9	1.1	1.3	2.5	0.5	1.8	0.7	0	81.6	82.8
	2	85.6	42.4	0.6	1.2	1.2	0.3	0.9	0.5	0	70.2	72.9
	3	80.9	46.9	0.6	1.3	1.6	0.3	0.9	0.5	0	77.0	80.3
	4	85.6	42.7	0.4	1.2	0.7	0.3	0.6	0.4	0	67.2	71.8
	5	77.2	48.5	0.6	1.3	0.8	0.3	0.8	0.5	0	76.5	81.7
	6	77.9	49.9	0.5	1.4	0.7	0.3	0.8	0.5	0	77.2	83.0
	7	87.4	45.4	0.4	1.2	0.3	0	0.4	0.4	0	69.5	73.1
	8	82.8	52.8	0.4	1.4	0.4	0	0.5	0.5	0	80.7	84.1
400	1	99	60.9	0.2	2.2	0.6	0.5	0.3	0.5	0	87.0	94.0
	2	98.9	46	0.2	1.4	0.3	0.2	0.2	0.5	0	69.1	70.6
	3	98.4	51.8	0.2	1.5	0.3	0.3	0.3	0.4	0	76.6	79.3
	4	96.6	54.9	0.2	1.6	0.4	0.4	0.4	0.4	0	81.7	84.6
	5	98.3	50.1	0.1	1.3	0.2	0.2	0.3	0.3	0	73.7	76.0
	6	97.9	50.2	0.1	1.3	0.2	0	0.2	0.3	0	73.3	75.9
	7	98.1	49.2	0.1	1.3	0.2	0	0.2	0.3	0	71.8	74.1

Mechanistic pathway of ethanol transformation

The ethanol to hydrocarbon conversion is quite complex and mainly based upon the understanding of methanol to hydrocarbon reaction. Different mechanistic investigations have been carried out over modified ZSM-5, SAPO, supported metal oxide etc. for both methanol to hydrocarbon (MTH) and ethanol to hydrocarbon (ETH) reactions [46]. Although there still lies some uncertainty regarding the actual reaction pathway but it is clear that both the reactions pass through the so-called hydrocarbon pool (HCP) mechanism. The hydrocarbon pool mechanism was originally proposed by Dahl and Kolboe using isotope labelling experiment for methanol reaction over H-SAPO-34 catalyst [47]. Also the subsequent investigation by Johansson et al. it was concluded that both methanol to gasoline (MTG) and ethanol to gasoline (ETG) result in same product distribution [48] as they mostly branch from similar mechanism. Further, computational investigations mainly suggested the HCP mechanism [49]. Accordingly there is no direct path from ethanol to detected products through C_2 entities but rather the zeolite with the entrapped HCP combined acts as an inorganic/organic scaffold for the formation of product by continuous rearrangement, addition and cracking of the HCP molecules. Ramasamy et al. performed ETH

reaction over HZSM-5 and concluded that at temperature above 300°C ethanol gets into a hydrocarbon pool mechanism, which associates continuous ethylation and results higher hydrocarbon compounds with water. After that these higher hydrocarbons gets involved in complex secondary reaction mechanisms like oligomerisation, cracking, isomerisation, dehydrocyclization to ultimately end up as a hydrocarbon mixture containing olefins, aromatics, paraffin, naphthene etc. [1]. Van der Borgh et al. carried out ETH reaction over metal modified ZSM-5 and proposed that ethylene can oligomerize to form higher hydrocarbons which can be cracked or subjected to H-transfer to ultimately form aromatics and paraffin. This direct ethanol to ethylene dehydration knocks out the requirement for an indirect C—C coupling route like the hydrocarbon pool mechanism [2]. In the ethanol to hydrocarbon conversion over metal supported alumina an alternative mechanism for the growth of hydrocarbon over M_xO_y nanoparticle ($\text{M} = \text{Re}, \text{W}, \text{Ta}$) has been proposed. Here the condensation reaction between ethanol and its intermediate reaction products predominantly yield C_3H_6 , C_4H_8 and C_6H_{12} alkenes. In case of Pt and Pd reductive dehydration occurs as a result of surface ethane condensation [3]. In case of supported metal oxides like NiO/MCM-41 ethylene is generated by dehydration of ethanol and then ethylene dimerization, isomerisation and metathesis

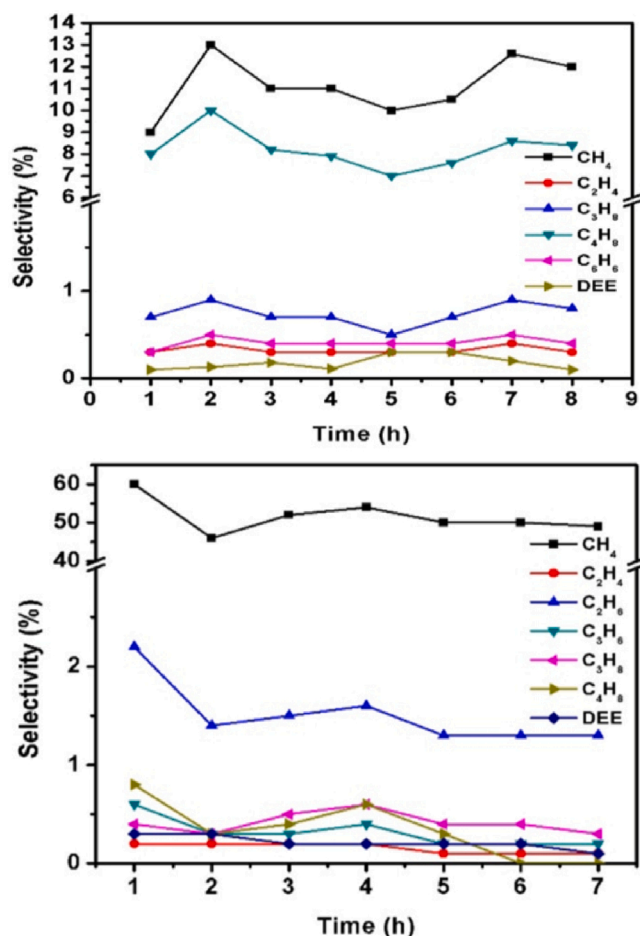
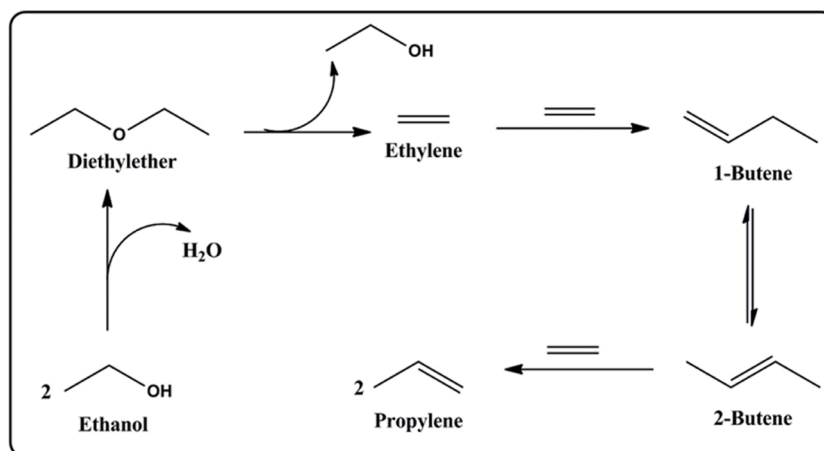


Fig. 6. Selectivity of reaction products for the dehydrogenation of ethanol over NiO@SBA-15 at 300 °C (top) and at 400 °C (bottom).

reactions follows [50]. Dehydration and isomerization takes place on the acidic silica support. On the other hand dimerization and metathesis takes place on the Ni site [51,52]. After considering all the possible mechanistic ways and the product distribution we can suggest a possible reaction pathway for ethanol to C₃-C₄ hydrocarbons over acidic NiO@SBA-15 catalyst as shown in Scheme 2.



Scheme 2. The schematic reaction pathway for the synthesis of hydrocarbons from ethanol.

Comparison with other reported catalysts

Ethanol conversion to hydrocarbons has been carried out over different catalytic systems, which mainly includes zeolites/modified zeolites and mixed metal oxides. Madeira et al. performed ethanol to hydrocarbon reaction over HZSM-5 catalyst at 350 °C temperature with a total pressure of 30 bar. They mainly obtained C₃₊ hydrocarbons in high selectivity and high conversion of ethanol [53]. Gayubo et al. carried out ethanol transformation to olefins on a Ni-ZSM-5 catalyst and also studied is deactivation [54]. They could achieve high selectivity for C₃-C₄ hydrocarbons at 400–500 °C temperature and 1 atm pressure with high conversion of ethanol. Iwamoto et al. reported complete ethanol conversion on Ni/MCM-41 catalyst with nearly 30 % selectivity for propylene at 400 °C with total pressure of 5.6 kPa [50]. Nikolaev et al. carried out conversion of ethanol to C₃₊ hydrocarbons over M/Al₂O₃ (M = NiO, Au, NiO/Au) catalysts at 350 °C temperature [3]. In case of the NiO cluster, it resulted a selectivity of 12.73 %, whereas for the mixed NiO/Au particles the selectivity increased up to 34.19 %. Ramasamy et al. carried out ethanol conversion over HZSM-5 catalyst at 300–400 °C at 300 psig and achieved complete ethanol conversion with high selectivity towards higher hydrocarbons [1]. In the investigation by Vander Brought et al., they prepared Ni, Ga, Fe modified ZSM-5 for ethanol to hydrocarbon reaction [2]. In terms of products they obtained light olefins, paraffins, aromatics and C₅₊ hydrocarbons at 350 °C temperature and 101 kPa total pressure over catalysts with low metal content. For most of the aforementioned catalytic systems for the ethanol to hydrocarbon reaction require high pressure conditions, where no pressure condition is needed for our synthesized NiO@SBA-15. On the other hand, though our higher hydrocarbon yield is low but there is substantial amount of hydrogen production which is impressive. Thus, our catalytic data suggested that NiO@SBA-15 is an efficient catalyst for the synthesis of renewable energy compounds from ethanol.

Experimental section

Synthesis of NiO@SBA-15

Pure silica SBA-15 have been synthesized by using triblock copolymer P123 as structure directing agent [39]. Then SBA-15 was surface modified with 3-aminopropyltriethoxysilane (APTES) to get F-SBA-15. 1.0 g SBA-15 was dispersed in 25 mL dry dichloromethane (DCM) and 0.728 g APTES was added to it followed by continuous stirring for 24 h. The reaction mixture was then filtered and washed with plenty of DCM and ethanol to obtain F-SBA-15. 1.0 g F-SBA-15 was then dispersed in 20 mL water and 0.324 g Ni(NO₃)₂ in 5 mL water was added to it. 1.0 mL NH₂-NH₂ was added dropwise for 10 min to the mixture and stirred for 4

h. The mixture was then filtered and washed with plenty of water to obtain Ni(II)@F-SBA-15. Then this Ni(II)@F-SBA-15 was calcined under air flow at 550 °C for 4 h to obtain NiO@SBA-15. Here during the catalyst synthesis NH_2NH_2 was used for successful binding of Ni(II) sites over the functionalized SBA-15. When we have carried out the immobilization in the absence of NH_2NH_2 , loading of Ni(II) at the mesopore surface was very poor.

Characterizations

Powder X-ray diffraction (PXRD) patterns were recorded by using a PANalytical X'Pert PRO diffractometer with $\text{Cu K}\alpha$ ($\lambda = 0.15406$ nm) radiation. The PXRD data in small angle was taken by using Bruker D-8 Advance diffractometer operated at 40 mA current using $\text{Cu K}\alpha$ ($\lambda = 0.15406$ nm) radiation and 40 kV voltage. We have calculated the particle size of the nanoparticles from powder X-ray diffraction FWHM data by using Scherrer's equation ($D = 0.89 \lambda / \beta \cos \theta$), where D is the mean size of the crystalline domain, λ is the $\text{Cu K}\alpha$ ($\lambda = 0.15406$ nm) radiation and β is the line broadening at half maxima intensity after subtracting the instrumental line broadening. A Quantachrome Autosorb-iQ system was used to do N_2 sorption analysis at liquid N_2 temperature 77 K. The samples were degassed at 150 °C under vacuum prior to the experiment. The non-local density function theory (NLDFT) method was used to obtain the average pore size distribution. The NH_3 -TPD measurement was carried out on a ChemiSorb 2750 instrument (Micromeritics, USA) using thermal conductivity detector. 100 mg material was activated under helium (99.999 %) gas flow at 623 K for 1 h and NH_3 was adsorbed at room temperature by flowing NH_3/He (10 %) at a rate of 25 mL/min before conducting the experiment. The TPD profile was recorded in the range of 310–1073 K under the flow of He (99.999 %).

Catalytic study

The catalytic reactions were carried out in a fixed bed tubular quartz reactor (9 mm i.d.) under atmospheric pressure using 200 mg of catalyst. The reaction temperature, measured by a thermocouple placed near the catalyst bed, was between 573 and 673 K. The catalyst bed was kept between a pair of glass wool block. Before the catalytic evaluation, the catalyst bed was preheated to eliminate water and other adsorbed species, using a N_2 flow (30 mL min^{-1}) at 723 K for 1 h (ramping rate: 5 K min^{-1}). When the catalyst bed was cooled down to reaction temperature, a 99.9 % ethanol was fed (through a pre-heater with temperature 473 K) at the top of the reactor with a syringe pump and mixed with a N_2 diluent (N_2 : EtOH mole ratio 5: 1). The WHSV (weight hourly space velocity) was $3.9 \text{ g}_{\text{EtOH}} \text{cat}^{-1} \text{ h}^{-1}$.

The gaseous effluent coming out from reactor after reaction was quantitatively analysed by an online gas chromatograph (Agilent 7890B gas chromatography) equipped with a capillary HP-PLOT Q column (30 m, 0.53 mm i.d.), and flame ionization detector. The yields of CO , CO_2 and H_2 were determined by Porapak Q packed column and 5A molecular sieve column present in the TCD. The carbon balance was calculated and respective catalytic activity results are shown in Table 1.

Conclusions

In summary, NiO NPs have been impregnated over 2D-hexagonally ordered mesoporous SBA-15 material and the resulting NiO@SBA-15 mesoporous catalyst has been characterized thoroughly by using PXRD, HR-TEM, XPS, NH_3 -TPD and N_2 sorption analyses. The material NiO@SBA-15 has been utilized as catalyst in fixed bed reactor for the transformation of ethanol into hydrocarbon fuels and hydrogen. It is observed that at 300 °C selectivity for the C4 product is higher and as temperature further increases pyrolysis process predominates over C4 hydrocarbon fuels. Utilization of biomass derived ethanol into lighter hydrocarbon fuels and hydrogen reported herein over NiO NPs

supported over 2D hexagonal mesoporous silica may open new opportunities for the utilization of supported 3d-transition metal oxides for the production of sustainable energy sources.

CRedit authorship contribution statement

Sauvik Chatterjee: Methodology, Data curation, Formal analysis, Writing - original draft. **Kushanava Bhaduri:** Methodology, Data curation, Formal analysis, Writing - original draft. **Arindam Modak:** Data curation, Formal analysis. **Manickam Selvaraj:** Data curation, Formal analysis. **Rajaram Bal:** Data curation, Formal analysis. **Biswajit Chowdhury:** Supervision, Funding acquisition, Writing - original draft, Writing - review & editing. **Asim Bhaumik:** Supervision, Funding acquisition, Writing - original draft, Writing - review & editing.

Declaration of Competing Interest

There are no conflicts to declare.

Acknowledgements

SC wishes to acknowledge DST, New Delhi, India for INSPIRE-SRF. The authors extend their appreciation to the Deanship of Scientific Research at King Khalid University for funding this study through the Small Research Group Project under grant number R.G.P. 306/1442. BC and AB wish to thank Indo-German Science & Technology Centre (IGSTC), New Delhi for an international collaboration project grant (CO2BioFeed). Authors would like to acknowledge Anirudha Singha for his help in product analysis.

Appendix A. Supplementary data

Supplementary material related to this article can be found, in the online version, at doi:<https://doi.org/10.1016/j.mcat.2020.111381>.

References

- [1] K.K. Ramasamy, Y. Wang, *Catal. Today* 237 (2014) 89–99.
- [2] K.V. der Borght, V.V. Galvita, G.B. Marin, *Appl. Catal. A Gen.* 492 (2015) 117–126.
- [3] S.A. Nikolaev, A.V. Chistyakov, M.V. Chudakova, E.P. Yakimchuk, V.V. Kriventsov, M.V. Tsodikov, *J. Catal.* 297 (2013) 296–305.
- [4] J.J. Lovón-Quintana, J.K. Rodríguez-Guerrero, P.G. Valença, *Appl. Catal. A Gen.* 542 (2017) 136–145.
- [5] A.K. Agarwal, *Prog. Energy Combust. Sci.* 33 (2007) 233–271.
- [6] M.K.D. Kiani, B. Ghobadian, T. Tavakoli, A.M. Nikbakht, G. Najafi, M.K. Deh Kiani, B. Ghobadian, T. Tavakoli, A.M. Nikbakht, G. Najafi, *Energy* 35 (2010) 65–69.
- [7] G.M. Chupka, E. Christensen, L. Fouts, T.L. Alleman, M.A. Ratcliff, R.L. McCormick, *SAE Int. J. Fuels Lubr.* 8 (2015) 251–263.
- [8] A. Taghizadeh-Alisaraei, A. Motevali, B. Ghobadian, *Renew. Energy* 143 (2019) 1094–1110.
- [9] N.M. Eagan, M.D. Kumbhalkar, J.S. Buchanan, J.A. Dumesic, G.W. Huber, *Nat. Rev. Chem.* 3 (2019) 223–249.
- [10] L. Cao, I.K.M. Yu, X. Xiong, D.C.W. Tsang, S. Zhang, J.H. Clark, C. Hu, Y.H. Ng, J. Shang, Y.S. Ok, *Environ. Res.* 186 (2020), 109547.
- [11] I. Staffell, D. Scamman, A.V. Abad, P. Balcombe, P.E. Dodds, P. Ekins, N. Shah, K. R. Ward, *Energy Environ. Sci.* 12 (2019) 463–491.
- [12] S.T. Wismann, J.S. Engbaek, S.B. Vendelbo, F.B. Bendixen, W.L. Eriksen, K. Aasberg-Petersen, C. Frandsen, I. Chorkendorff, P.M. Mortensen, *Science* 364 (2019) 756–759.
- [13] Y. Lin, S. Tanaka, *Appl. Microbiol. Biotechnol.* 69 (2006) 627–642.
- [14] S. De, B. Saha, R. Luque, *Bioresour. Technol.* 178 (2015) 108–118.
- [15] C. Wang, Y. Wang, M. Chen, J. Hu, Z. Yang, H. Zhang, J. Wang, S. Liu, *Int. J. Hydrog. Energy* 44 (2019) 26888–26904.
- [16] C. Mondelli, G. Gozaydin, N. Yan, J. Perez-Ramirez, *Chem. Soc. Rev.* 49 (2020) 3764–3782.
- [17] C. Perego, R. Millini, *Chem. Soc. Rev.* 42 (2013) 3956–3976.
- [18] K.B. Baharudin, Y.H. Taufiq-Yap, J. Hunns, M. Isaacs, K. Wilson, D. Derawi, *Microporous Mesoporous Mater.* 276 (2019) 13–22.
- [19] S.K. Das, S. Chatterjee, S. Mondal, A. Bhaumik, *Mol. Catal.* 475 (2019), 110483.
- [20] S. Rostamnia, N. Nouruzi, H. Xin, R. Luque, *Catal. Sci. Technol.* 5 (2015) 199–205.
- [21] E. Doustkhah, J. Lin, S. Rostamnia, C. Len, R. Luque, X. Luo, Y. Bando, K.C.-W. Wu, J. Kim, Y. Yamauchi, Y. Ide, *Chem. Eur. J.* 25 (2019) 1614–1635.
- [22] E. Doustkhah, H. Mohtasham, M. Hasani, Y. Ide, S. Rostamnia, N. Tsonoji, M.H. N. Assadi, *Mol. Catal.* 482 (2020), 110676.
- [23] T. Yokoi, T. Tatsumi, H. Yoshitake, *J. Colloid Interface Sci.* 274 (2004) 451–457.

- [24] S. Verma, M. Nandi, A. Modak, S.L. Jain, A. Bhaumik, *Adv. Synth. Catal.* 353 (2011) 1897–1902.
- [25] W. Chen, X. Li, Z. Pan, S. Ma, L. Li, *Chem. Eng. J.* 304 (2016) 594–601.
- [26] J. Liang, Z. Liang, R. Zou, Y. Zhao, *Adv. Mater.* 29 (2017), 1701139.
- [27] Y. Jia, Z.A. Allothman, R. Liang, S. Cha, X. Li, W. Ouyang, A. Zheng, S.M. Osman, R. Luque, Y. Sun, *Mol. Catal.* 495 (2020), 111146.
- [28] S. Singh, R. Kumar, H.D. Setiabudi, S. Nanda, D.V.N. Vo, *Appl. Catal. A Gen.* 559 (2018) 57–74.
- [29] S. Rojas-Buzo, P. Garcia-Garcia, A. Corma, *Catal. Sci. Technol.* 9 (2019) 146–156.
- [30] T.H. Truong, V.C. Do, N.M. Do, T.Q. Hung, H.V. Doan, T.N. Nguyen, T.H. Doan, T. H.N. Le, T.V. Nguyen, L.G. Bach, Q.V. Tran, *Mol. Catal.* 478 (2019), 110571.
- [31] L. Paul, S. Mukherjee, S. Chatterjee, A. Bhaumik, D. Das, *ACS Omega* 4 (2019) 17857–17863.
- [32] A.C. Gujar, V.K. Guda, M. Nolan, Q. Yan, H. Toghiani, M.G. White, *Appl. Catal. A Gen.* 363 (2009) 115.
- [33] Z. Song, A. Takahashi, I. Nakamura, T. Fujitani, *Appl. Catal. A Gen.* 384 (2010) 201–205.
- [34] Z. Wang, L.A. O'Dell, X. Zeng, C. Liu, S. Zhao, W. Zhang, M. Gaborieau, Y. Jiang, J. Huang, *Angew. Chem. Int. Ed.* 58 (2019) 18061–18068.
- [35] J. Bi, M. Liu, C. Song, X. Wang, X. Guo, *Appl. Catal. B Environ.* 107 (2011) 68–76.
- [36] V.F. Tretyakov, Y.I. Makarfi, K.V. Tretyakov, N.A. Frantsuzova, R.M. Talyshinskii, *Catal. Ind.* 2 (2010) 402–420.
- [37] S. Mondal, A. Sen, *ACS Appl. Energy Mater.* 2 (2019) 2398–2401.
- [38] Y. Perez, I. del Hierro, L. Zazo, R. Fernandez-Galan, M. Fajardo, *Dalton Trans.* 44 (2015) 4088–4101.
- [39] Y. Hailong, Z. Deyang, J. Xu, Y. Lu, Y. Liu, K. Qiu, Y. Zhang, Y. Lao, *Nanoscale Res. Lett.* 9 (2014) 424.
- [40] P. Bhanja, A. Modak, S. Chatterjee, A. Bhaumik, *ACS Sustain. Chem. Eng.* 5 (2017) 2763–2773.
- [41] U. Kayal, B. Mohanty, P. Bhanja, S. Chatterjee, D. Chandra, M. Hara, B.K. Jena, A. Bhaumik, *Dalton Trans.* 48 (2019) 2220–2227.
- [42] D.Y. Zhao, J.Y. Sun, Q.Z. Li, G.D. Stucky, *Chem. Mater.* 12 (2000) 275–279.
- [43] W. Huang, S. Ding, Y. Chen, W. Hao, X. Lai, J. Peng, J. Tu, Y. Cao, X. Li, *Sci. Rep.* 7 (2017) 5220.
- [44] C.C. Chong, S.N. Bukhari, Y.W. Cheng, H.D. Setiabudi, A.A. Jalil, *Appl. Catal. A Gen.* 584 (2019), 117174.
- [45] H. Sohn, U.S. Ozkan, *Energy Fuels* 30 (2016) 5309–5322.
- [46] U. Olsbye, S. Svelle, M. Bjorgen, P. Beato, T.V.W. Janssens, F. Joensen, S. Bordiga, K.P. Lillerud, *Angew. Chem. Int. Ed.* 51 (2012) 2–24.
- [47] M. Dahl, S. Kolboe, *J. Catal.* 161 (1996) 304–309.
- [48] R. Johansson, S.L. Hruby, J. Rass-Hansen, C.H. Christensen, *Catal. Lett.* 127 (2009) 1–6.
- [49] D. Dumer, K. Ruchle, W. Reschetilowski, *ChemCatChem* 4 (2012) 802–806.
- [50] M. Iwamoto, K. Kasai, T. Haishi, *ChemSusChem* 4 (2011) 1055–1058.
- [51] M. Iwamoto, Y. Kosugi, *J. Phys. Chem. C* 111 (2007) 13–15.
- [52] S. Sugiyama, Y. Kato, T. Wada, S. Ogawa, K. Nakagawa, K.-I. Sotowa, *Top. Catal.* 53 (2010) 550–554.
- [53] F. Ferreira Madeira, N.S. Gnep, P. Magnoux, H. Vezin, S. Maury, N. Cadran, *Chem. Eng. J.* 161 (2010) 403–408.
- [54] A.G. Gayubo, A. Alonso, B. Valle, A.T. Aguayo, M. Olazar, J. Bilbao, *Chem. Eng. J.* 167 (2011) 262–277.